INL/JOU-21-63599-Revision-0

Nature of Oxygen Adsorption on Defective Carbonaceous Materials

September 2021

Zongtang Fang, Rebecca R Fushimi, Eric J Dufek, Lan Li, David Dixon

Changing the World's Energy Future

Idaho National Laboratory

INL is a U.S. Department of Energy National Laboratory operated by Battelle Energy Alliance, LLC

INL/JOU-21-63599-Revision-0

Nature of Oxygen Adsorption on Defective Carbonaceous Materials

Zongtang Fang, Rebecca R Fushimi, Eric J Dufek, Lan Li, David Dixon

September 2021

Idaho National Laboratory
Idaho Falls, Idaho 83415

http://www.inl.gov

Prepared for the
U.S. Department of Energy
Under DOE Idaho Operations Office
Contract DE-AC07-05ID14517

THE JOURNAL OF PHYSICAL CHEMISTRY C
A JOURNAL OF THE AMERICAN CHEMICAL SOCIETY

pubs.acs.org/JPCC

Article

Nature of Oxygen Adsorption on Defective Carbonaceous Materials

Zongtang Fang,* Lan Li, David A. Dixon, Rebecca R. Fushimi, and Eric J. Dufek*

Cite This: https://doi.org/10.1021/acs.jpcc.1c06741

Read Online

ACCESS | Metrics & More | Article Recommendations | Supporting Information

ABSTRACT: Plane-wave density functional theory has been used to study oxygen adsorption on graphene, graphite, and (12,0) zigzag single-walled carbon nanotubes with and without Stone−Wales (SW) and single-vacancy (SV) defects to understand the role of defects on carbonaceous material reactivity. Atomic oxygen adsorption leads to the formation of an epoxide on defect-free graphene and graphite and an ether on the exterior wall of carbon nanotubes and SW-defected materials. O_2 chemisorption is endothermic on defect-free graphene and graphite and slightly exothermic on defect-free nanotubes. O_2 chemisorption energies are predicted to be −1.1 to −1.4 eV on an SW defect and −6.0 to −8.0 eV on an SV defect. An SW defect lowers the energy barriers by 0.90 and 0.50 eV for O_2 chemisorption on graphene and nanotubes, respectively. The formation of a C−O−O−C group is important for O_2 dissociation on defect-free and SW-defected materials. The energy barrier is less than 0.30 eV on an SV defect. The more reactive SW defect toward O adsorption on graphene is mostly due to the strained defective carbon atoms being able to donate more electrons to an O to form an ether. The larger 2s character in the hybrid orbitals in an ether than in an epoxide makes the ether C−O bond stronger. Stronger C−O binding on an SW-defective carbon nanotube than on a defect-free nanotube is in part due to more flexibility of the defect to release the epoxide ring strain to form an ether.

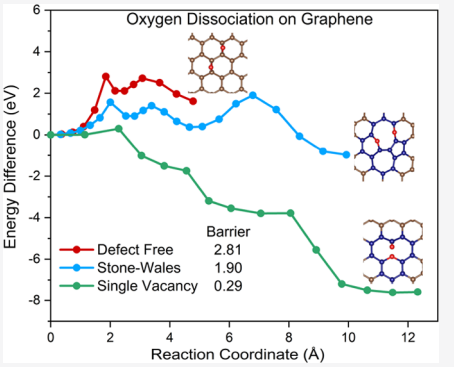

INTRODUCTION

Carbon materials such as graphene, graphite, nanotubes, and fullerene-related materials have been widely used for gas adsorption and storage,[1,2] catalysis,[3−5] and battery anodes.[6] These materials have properties that are often associated with carbon's ability to change hybridization from sp to sp^3. Hybrid carbon phases also exist in combinations of hybridized atomic orbitals, such as sp^2 + sp^3.[7,8] Graphite with sp^2 hybridization is the most stable form of carbon under standard conditions.[9] Deformed sp^2 hybridization may lead to the formation of curvatures of carbonaceous materials such as found in carbon nanotubes.[10] Non-sp^2 hybrid carbon atoms are also the origin of intrinsic defects such as the Stone−Wales (SW) defect, single-vacancy (SV) defect, and multiple vacancy defects.[11] A Stone−Wales defect includes two pairs of five-membered and seven-membered rings formed by rotating a C−C bond in a six-membered ring by 90°.

Defected carbonaceous materials exhibit novel mechanical, electrical, and chemical properties and have played an important role in the field of catalysis and energy storage.[12−20] Defective graphite or graphitized material-supported nanoparticles, clusters, or single atoms have been used in a wide range of catalytic reactions including hydrogenation, hydrogenolysis, dehalogenation, and the oxygen evolution reaction (OER).[21−23] A computational study of CO and O_2 adsorption on single gold atoms supported on defected single-walled carbon nanotubes (SWCNT) showed that the defects improved the binding strength of the Au−C bond as well as improving the catalytic activity.[20] In addition, more charge transfer from gold to O_2 was predicted on the defected SWCNT compared to that on the pristine SWCNT.[20] Carbon defects in defected carbon spheres were reported to be active in electrocatalytic CO_2 reduction, and an increase in defect concentration could enhance catalytic performance.[13]

Among those applications, the adsorption of oxygen on carbonaceous materials is critical in oxidative dehydrogenation,[24,25] the oxygen evolution reaction,[26] and the oxygen reduction reaction.[27,28] The reaction of molecular oxygen with the highly oriented pyrolytic graphite (HOPG) (001) surface at 1000 K was studied using X-ray absorption spectroscopy (XAS), and the electronic structure of the studied material with a 10% weight loss remained unchanged.[29] A computational study of oxygen adsorption on graphite and the (8,0) SWCNT predicted epoxide formation and that chemisorption of an oxygen molecule was not energetically favorable on graphite and the interior surface of the SWCNT.[30] In comparison, chemisorption was slightly exothermic on the exterior surface of the SWCNT. Additional theoretical studies on the oxygenation of perfect SWCNT also predicted the

Received: July 29, 2021

formation of an epoxy structure.[31,32] Lee et al. reported that the molecular oxygen chemisorption was exothermic at the top sites and/or the bridge sites of a vacancy on graphite using scanning tunneling microscopy (STM) in combination with density functional theory (DFT) calculations.[33] Another computational study of oxygen adsorption on a vacancy defect as well as B- and N-doped nuclear graphite predicted that the defective graphite was more sensitive to O_2 than perfect graphite. Interestingly, the substitution of B and N improved the oxygen resistance of nuclear graphite.[34]

Although oxygen adsorption on some defective carbonaceous materials has been reported,[33,34] the detailed reaction pathways of molecular oxygen dissociation on the defective carbon atoms remain unknown. The difference in the binding nature of an oxygen bonded to a perfect surface or to a defective surface is still not established. In the current work, molecular and atomic oxygen adsorption on defective carbonaceous materials was studied using plane-wave DFT to investigate how the defects affect surface reactivities. Stone−Wales and single-vacancy defects were introduced into graphene, graphite, and (12,0) zigzag single-walled carbon nanotubes. The carbon nanotubes were selected to study the role that curvature plays on the oxygen reactivity. Similar reactions on defect-free materials were also calculated for comparison. To better understand the composition of the natural hybrid orbitals and the natural C−O bonds in the epoxide and ether, oxygen adsorption on graphene and carbon nanotube with and without an SW defect using cluster models was further investigated. The cluster calculations were performed using atomic basis functions.

COMPUTATIONAL METHOD

Structure relaxations for graphene and carbon nanotubes were carried out at the density functional theory (DFT) level with the Perdew−Burke−Ernzerhof (PBE) exchange-correlation functional[35] using the Vienna ab initio simulation package (VASP).[36−38] The spin-polarized DFT calculations with a cutoff energy of 400 eV were performed using plane-wave basis sets and the projector-augmented wave (PAW) pseudopotentials. The PBE functional was chosen as it worked well in previous calculations on both graphene and nanotubes because the predicted C−C bond distance with PBE is consistent with the experiment and there are no interlayer interactions for graphene and nanotubes.[32,34,39,40] The van der Waals corrections are needed for the calculations on graphite and the graphite calculations were carried out using the optimized optPBE-vdw[41] functional using the same basis functionals with a cutoff energy of 420 eV. The interlayer distance in the graphite crystal with PBE is predicted to be 3.467 Å, which is 0.12 Å larger than the experimental value of 3.35 Å;[42] whereas the optPBE-vdw functional gives a value of 3.34 Å, in better agreement with the experiment. Both PBE and optPBE-vdw functionals predict the C−C bond distance to be 1.42 Å, which is consistent with the experiment. A cutoff energy of 420 eV was selected for the calculations using the optPBE-vdw functional as the predicted interlayer distance of 3.27 Å in graphite using a cutoff energy of 400 eV is slighter shorter than the value of 3.34 Å using a cutoff energy of 420 eV and the experiment. Additionally, the test results for the atomic oxygen adsorption energies on the basal plane of defect-free graphite are the same using the cutoff energies of 420 and 400 eV with optPBE-vdw. Selected calculations show that the exothermicity of atomic oxygen adsorption on SW-defected graphite could be overestimated by 0.4 eV with PBE compared to that with optPBE-vdw. Oxygen adsorption reactions for graphene were also calculated with the optPBE-vdw functional for a direct comparison to the results on graphite to study how graphene layers affect the oxygen reactivity on the basal plane.

The graphene layer was modeled by a 6 × 6 supercell including 72 carbon atoms, as shown in Figure S1, and a 3 × 3 × 1 Γ-centered Monkhorst−Pack k-point grid was used for the surface calculations. Three graphene layers were built to model the reactions on the basal plane of graphite. The vacuum distance between two slabs was set to 20 Å. The bottom layer was fixed, and the top two graphene layers were relaxed in the calculations. Additional calculations using more graphene layers gave approximately the same oxygen adsorption energy as using three graphene layers (Figure S2). A computational model including 192 carbon atoms with a diameter of 9.47 Å was selected for the (12,0) zigzag single-walled carbon nanotubes. A 1 × 1 × 5 k-point mesh was selected, and all atoms were relaxed in the calculations of the nanotube. The vacuum distance between the two carbon nanotubes was 15 Å to avoid the interactions between two images. Only the adsorption on the exterior wall of the nanotube was studied to compare the results on the surfaces of graphene and graphite. For the defective materials, either an SW defect or an SV defect was introduced in the middle region of the slab (Figure S1).

Structure relaxations were performed until the residual force on each atom was less than 0.02 eV/Å. The adsorption energy (E_{ads}) at 0 K was calculated using eq 1

$$\Delta E_{ads} = E_{slab+on} - E_{slab} - n/2 \times E_{O_2} \quad (1)$$

where $E_{slab+on}$ and E_{slab} are the total electronic energies of the surface slab with and without the adsorbate of an O_2 molecule or an O atom; E_{O2} is the electronic energy of the gas-phase oxygen molecule, which was calculated with an 8.0 Å × 8.0 Å × 8.0 Å unit cell at the γ point only. One-half of the electronic energy of O_2 was selected as the reference to study oxygen adsorption at the lowest surface coverage. The electronic energies for different species in eq 1 are from the calculations using the same cutoff energy. The climbing image nudged elastic band (cNEB) method[43,44] was used to locate transition states for oxygen dissociative chemisorption. The local charges of the atoms were calculated with a Bader charge analysis.[45,46]

The composition of the hybrid orbitals was determined using NBO6[47,48] for a natural bond orbital (NBO)[49−52] analysis for the cluster model. A 5 × 5 × 1 unit cell (70 carbon atoms) from the graphite crystal with H atoms attached to the terminal C atoms was selected to model graphene. For the nanotube, we selected a system containing 144 carbon atoms with H atoms attached to the terminal C atoms. The atomic oxygen adsorption energies on defect-free materials using a large cluster model ($C_{96}H_{26}$ for the graphene and $C_{192}H_{24}$ for the nanotube) differ by only 0.05 eV (Figure S7). An SW defect was introduced to study the binding nature of different C−O bonds in the epoxide and ether. Geometry optimizations were performed using the M06-2X exchange-correlation functional[53] with modest 6-31G basis sets[54−56] for C, O, and H. Single-point energy calculations using the 6-311G(d,p)[54−56] basis set with the M06-2X functional were then performed. The M06-2X functional was selected as it described the electron polarization densities well in graphene and carbon nanotube systems[57] and the electron densities are important for the NBO analysis. The calculated vibrational frequencies of

https://doi.org/10.1021/acs.jpcc.1c06741
J. Phys. Chem. C XXXX, XXX, XXX−XXX

the global minimum are employed to obtain the zero-point energy corrections (ZPEs). The open-shell DFT calculations were carried out in the spin-unrestricted formalism. The DFT calculations on the clusters were performed using Gaussian 16.[58] The atomic oxygen adsorption energies are calculated using one-half of the electronic energy of molecular oxygen as the reference to be consistent with the periodic calculations.

RESULTS AND DISCUSSION

Atomic Oxygen Adsorption. The adsorption of a triplet oxygen atom on the most favorable sites was first investigated and the results are shown in Figure 1 and Table S1. The

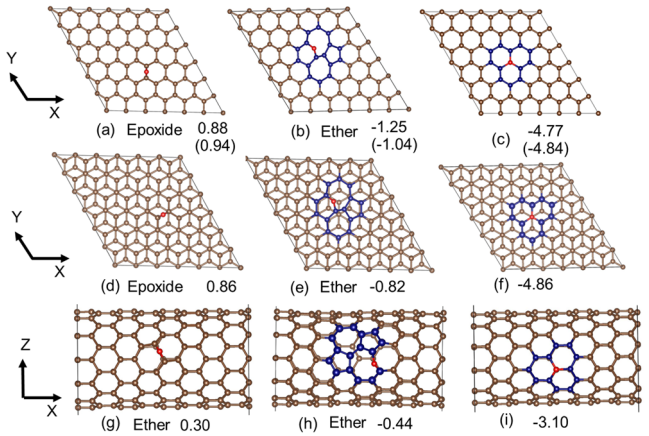

Figure 1. Top views of atomic oxygen adsorption on the basal planes of defect-free (a, d), SW-defected (b, e), and SV-defected (c, f) graphene and graphite. Side views of atomic oxygen adsorption on defect-free (g), SW-defected (h), and SV-defected (i) (12,0) zigzag single-walled carbon nanotubes. Adsorption energies are shown in eV with optPBE-vdw for graphene and graphite and with PBE for the nanotube. The PBE values for graphene are also shown in the parenthesis for comparison; O shown in red, C shown in brown, and the defective carbon atoms shown in blue.

structures and adsorption energies predicted with the optPBE-vdw functional for graphene and graphite and with the PBE functional for nanotubes are used in the following discussion unless otherwise noted. It is important to note that one-half of the electronic energy of O_2 was selected as the reference to calculate atomic oxygen adsorption energies. Oxygen adsorption on defect-free materials is studied for comparison purpose and the adsorption on defective materials is the primary focus in the current work. The total magnetic moment is zero for the defect-free and SW-defected materials as well as the products with oxygen adsorption. A triplet state of the product for atomic oxygen adsorption on defect-free graphene is predicted to be 1.0 eV higher in energy per unit cell than the singlet. At an SV defect on graphene and graphite, there are two unpaired electrons on two of the bi-coordinated carbon atoms, respectively. There is approximately one unpaired electron on a bi-coordinated carbon around an SV defect on the nanotube. The extra spin is paired with the chemisorbed oxygen for all SV-defected materials.

On graphene, the optPBE-vdw functional gives slightly less endothermic or more exothermic adsorption energies than the PBE functional. On defect-free graphene, the oxygen is bonded to two carbon atoms with the formation of an epoxy group and all of the carbon bridge sites are identical for oxygen adsorption (Figure 1a). The ∠C−O−C of the epoxide is predicted to be 62.0°. The existence of an SW defect lowers the atomic oxygen adsorption energy by ∼2 eV (Figure 1b). The most exothermic adsorption site is bridging a C−C bond between a five- and a seven-membered ring, leading to the formation of an ether-type product. The ∠C−O−C in the ether group is 102.9°. On the basal plane with an SV defect, the adsorbed oxygen atom occupies the vacant site and is bonded to adjacent three carbon atoms with a binding energy of −4.84 eV (Figure 1c). The three carbon atoms form a plane including the central oxygen with a bond angle of 120° for each ∠C−O−C. The predicted structures and energetics at the PBE level for atomic oxygen adsorption on defect-free and the SV-defected graphene are generally consistent with the previous studies at the same level.[40,59] With the presence of an SW defect, the adsorption energy on the most favorable bridge site with the formation of an ether is consistent with the previous results using a 5 × 5 supercell using the PBE functional with and without dispersion corrections.[40] Either an ether or an epoxide can be formed depending on the binding sites around the SW defect and the details are shown in the following section.

The results for the atomic oxygen adsorption on graphite modeled by three graphene layers are also shown in Figure 1d−f. The most favorable adsorption sites on the defect-free and the defective graphite are consistent with that on single-layer graphene. Less negative adsorption energies are predicted on the defected graphite, and the difference of adsorption energies on graphene and graphite is generally <0.4 eV.

On (12,0) carbon nanotubes, ether-like structures are predicted for the oxygen adsorption on both a defect-free surface and a defective surface in the presence of an SW defect (Figure 1g,h). Consistent with the previous work on (10,0) defect-free nanotubes,[60] O adsorption on the bridge site of an axis C−C bond with the formation of an epoxide is more endothermic by 0.15 eV as compared to that on a zigzag C−C bond, where ether formation is favored. The presence of an SW defect lowers the adsorption energy by 0.7 eV (Figure 1h). The ∠C−O−C in the ether group on a defect-free exterior wall is slightly smaller than that on an SW defect site. On the SV site, the adsorbed oxygen does not form a plane with the three adjacent carbon atoms, and the ∠C−O−C is slightly less than 120°. The oxygen adsorption energy on the SV defect site of the nanotube is ∼1.7 eV less negative than that on graphene and graphite.

On the surface with an SW defect, there exist multiple different adsorption sites around the defective carbon atoms, leading to different adsorption energies. Bader charge analysis can be used to further understand the interaction between the atomic oxygen and different surface carbon atoms. The plot of oxygen adsorption energies on various adsorption sites versus the Bader charges of adsorbed oxygen atoms is shown in Figure 2. Epoxide formation is favored on the active sites of a five-membered ring. A bridge site between the two seven-membered rings giving the formation of an epoxide is consistent with the previous results using an slab[61] and a cluster model.[59] Slightly more exothermic adsorption is predicted on the graphene and graphite than that on the (12, 0) nanotube. The net charges of the oxygen atoms are predicted to be mostly consistent with a value of −0.8 e in the different epoxides. The adsorption energies with the formation of epoxides range from −0.75 to 0.5 eV. Comparatively, more negative charges of the oxygen atoms ranging from −1.05 e to −1.10 e in the ethers are found. The adsorption leading to the

https://doi.org/10.1021/acs.jpcc.1c06741
J. Phys. Chem. C XXXX, XXX, XXX−XXX

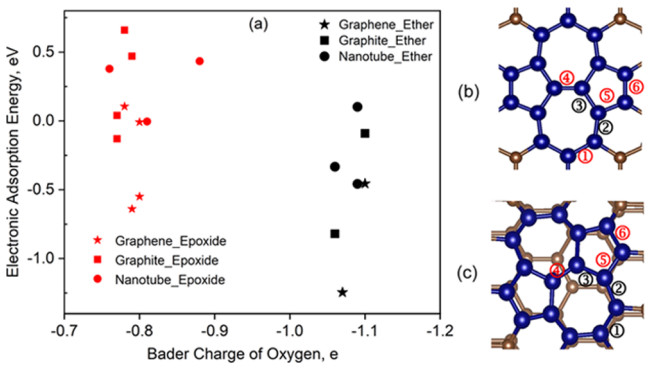

Figure 2. Oxygen adsorption energies on various sites around an SW defect versus the Bader charges of oxygen atoms in both epoxides and ethers (a). Multiple different adsorption sites on the SW defect on the graphene, graphite (b), and nanotube (c). Note: Adsorption energies are shown in eV with optPBE-vdw for graphene and graphite and with PBE for the nanotube. In (b) and (c), the site with a black number gives an ether formation in oxygen adsorption and epoxide formation is favored at the other sites (the numbers shown in red); (b) the adsorption sites on both graphene and graphite as the adsorption sites on the basal plane of graphite are consistent with that on graphene and only the top layer is shown for clarity for the graphite. Detailed structures and energetics are shown in Figure S3.

formation of an ether also has different adsorption energies on different binding sites, and their energies differ by up to 0.70 eV. Although the charge transfers from the surface to the oxygen for the formation of either an epoxide or an ether on different sites are comparable, the adsorption energies are calculated to be significantly different. Such energy differences suggest that the overlap of the hybrid orbitals from C and O plays an important role in the C−O binding strength and neither the epoxy nor the ether group has unpaired electrons.

Molecular Oxygen Adsorption. *Physisorption.* The physisorption of an oxygen molecule on defect-free and defective carbon materials (Figure S4) is mostly driven by Van der Waals interactions, and the corresponding physisorption energies are less negative than −0.6 eV with the optPBE-vdw functional. Each of the oxygen atoms in the physisorbed adducts has one unpaired spin, consistent with the spin on the molecule. The dispersion contributes to ∼0.2 eV for the O_2 physisorption energy. On the basal plane of defect-free graphene and graphite, the physisorption energies are predicted to be only −0.24 and −0.37 eV. Our calculated O_2 physisorption energy on defect-free graphene with PBE (−0.03 eV, Figure S4) is consistent with the previously reported value of −0.01 eV using a periodic model with the same functional[62] and using a cluster model with the B3LYP functional.[63] On the exterior wall of defect-free nanotubes, the calculated physisorption energy is −0.21 eV. Slightly stronger interactions between molecular oxygen and the SW-defected graphene and graphite are predicted and the adsorption energies are −0.51 and −0.45 eV, respectively. A slight distortion of the basal plane is predicted along with O_2 physisorption. The binding energy is 0.23 eV for O_2 physisorption on the nanotube with an SW defect. For the SV-defected graphene and graphite, the calculated adsorption energies are −0.41 and −0.20 eV. The addition of an oxygen molecule to the nanotube with an SV defect forms a C−O bond with a defective carbon atom with an adsorption energy of −0.47 eV. That C−O bond distance is calculated to be 1.36 Å. These binding energies are low so that O_2 is unlikely to physisorb at 298 K as the entropy of free O_2 at 298 K is 49 cal/mol-K giving a $T\Delta S$ term of 0.63 eV.

Dissociative Chemisorption. The structures and energetics for the oxygen chemisorption are shown in Figure 3. The total

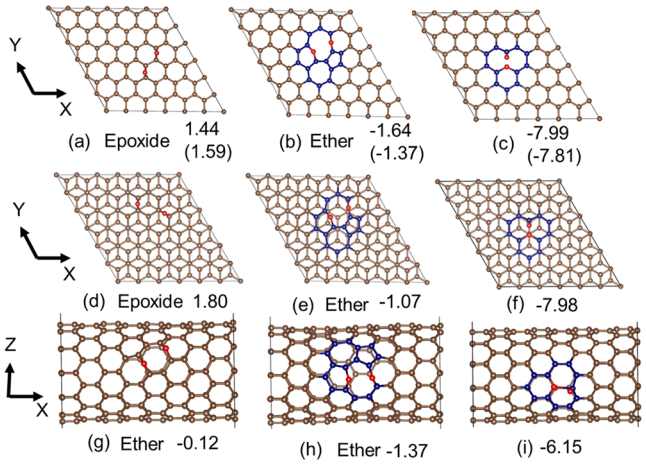

Figure 3. Top views of oxygen chemisorption on the basal planes of defect-free (a, d), SW-defected (b, e), and SV-defected (c, f) graphene and graphite. Side views of oxygen chemisorption on defect-free (g), SW-defected (h), and SV-defected (i) (12,0) zigzag single-walled carbon nanotubes. Adsorption energies are shown in eV with optPBE-vdw for graphene and graphite and with PBE for the nanotube. The PBE values for graphene are shown in parenthesis. See Figure 1 caption for the colors of atoms.

magnetic moment is zero for the chemisorption products. The addition of an oxygen molecule on graphene leads to the formation of two epoxy groups (Figure 3a). This step is endothermic by 1.44 eV. In comparison, the chemisorption of molecular oxygen on the grapheme with an SW defect is exothermic by −1.64 eV. Instead of forming two epoxy groups on a perfect surface, the formation of two ether groups is predicted around the SW defect. The most exothermic structure is the one including two ether groups on two sides of a seven-membered ring (Figure 3b). Additional adsorption configurations are shown in Figure S5. The adsorption leading to the formation of a mixture of an ether group and an epoxy group or two epoxy groups is either less exothermic or endothermic. On graphene with an SV defect, the oxygen chemisorption leads to the formation of an ether group on the basal plane with two defective bi-coordinated carbon atoms and a dangling C−O bond with the third bi-coordinated defective carbon atom (Figure 3c). This is much more exothermic compared to the chemisorption on defect-free and SW-defected graphene. The preference of forming an epoxide on the defect-free structure and one pair of ether and carbonyl groups on the SV-defected sites is consistent with the previous studies with photoelectron spectroscopy[64,65] and DFT calculations on graphitic materials.[65] This dissociation energy is also comparable to that on a four-atom (V4) vacancy on graphene, where the formation of two ether groups was predicted with PBE.[66]

The dissociative chemisorption of an oxygen molecule on graphite is more endothermic or less exothermic as compared to that on graphene. The calculated dissociation energies on graphene and graphite differ by 0.36, 0.57, and 0.01 eV on a defect-free, an SW-defected, and an SV-defected basal plane, respectively (Figure 3d,f). Again, the $T\Delta S$ for a free O_2 makes

https://doi.org/10.1021/acs.jpcc.1c06741
J. Phys. Chem. C XXXX, XXX, XXX−XXX

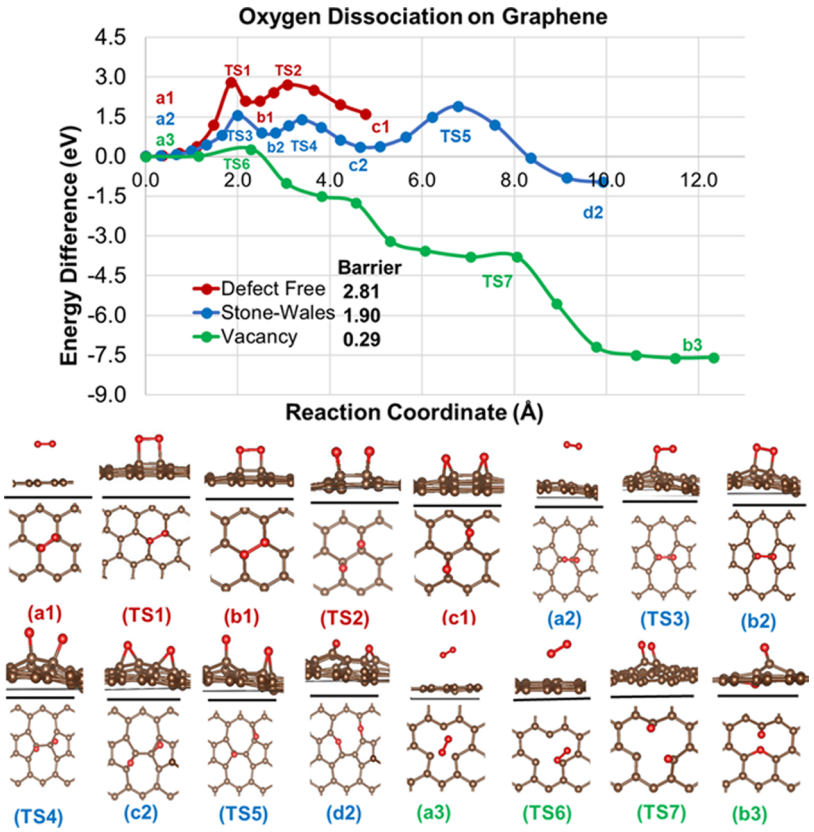

Figure 4. Calculated oxygen dissociation pathways on defect-free, SW-defected, and SV-defected graphene at the PBE level. The side-view structures are shown at the top and the top views are shown at the bottom. Note: only local structures are shown and the colors for the defective and normal carbon atoms are the same. The green and blue pathways on the defective graphene are exothermic.

it unlikely that the species on defect-free graphite will exist at equilibrium at 298 K.

On the exterior wall of the defect-free carbon nanotube, the oxygen chemisorption leading to the formation of two ether groups (Figure 3g) instead of the epoxy groups formed on defect-free graphene and graphite is predicted. Surprisingly, this chemisorption is slightly exothermic by −0.12 eV. This is partially due to the surface curvature, which provides somewhat structural flexibility to avoid the ring strain in a relatively less stable epoxide formed on the defect-free graphene. On an SW defect, the most stable configuration with two ether groups formed in a seven-membered ring (Figure 3h) agrees well with that on SW-defected graphene and graphite. The predicted chemisorption energy of −1.37 eV is less exothermic than that on graphene and more exothermic than that on graphite. The most stable configuration for oxygen chemisorption on the SV-defected carbon nanotube (Figure 3i) is similar to that on the SV-defected graphene and graphite. An exothermic energy of −6.19 eV is predicted.

Oxygen Dissociation Pathway. The significantly different chemisorption energies on the defect-free and the defective materials shown above suggest that molecular oxygen could be activated by a defect under mild conditions. The detailed oxygen dissociation pathways on the defective materials were studied by a series of activation energy calculations. Transition-state calculations on defect-free materials were also investigated for comparison. As the most stable chemisorption products on graphene and graphite are the same and the chemisorption energies are comparable, our studies only focus on the dissociation pathway on the graphene. The potential energy surfaces for O_2 dissociation starting from the physisorbed structures for graphene and nanotubes at the PBE level are shown in Figures 4 and 5, respectively. It is important to note that the chemisorption pathway includes multiple intermediate steps. The total magnetic moment is zero for all of the intermediates and the final products. Unpaired electrons may exist for the transition states depending on the materials.

On defect-free graphene, the formation of two epoxy groups in molecular oxygen chemisorption is predicted to pass through an intermediate with a C−O−O−C group (b1 in Figure 4). This step includes a spin crossing from the triplet to the singlet state for the O_2 adsorbate with a barrier energy of 2.81 eV. The adsorbed oxygen atoms as well as the carbon atoms in the transition state are in the singlet state with zero magnetic moments. An epoxide is formed by breaking the peroxyl −O−O− bond followed by the transfer of two oxygen adatoms to adjacent bridge C−C sites. The second transition state has a lower energy than the first, and the formation of a surface C−O−O−C group is the rate-limiting step. There are no unpaired electrons for the second transition state. This reaction mechanism for O_2 dissociation on defect-free graphene is consistent with a previous report[39] with the PBE functional and the predicted barrier energies differ by only 0.10 eV.

A different mechanism is predicted for oxygen dissociation on the SW-defected graphene. The formation of two ether groups includes three steps, and the first two steps are similar to that for oxygen dissociation on the perfect graphene. The production of an intermediate including a C−O−O−C group

https://doi.org/10.1021/acs.jpcc.1c06741
J. Phys. Chem. C XXXX, XXX, XXX−XXX

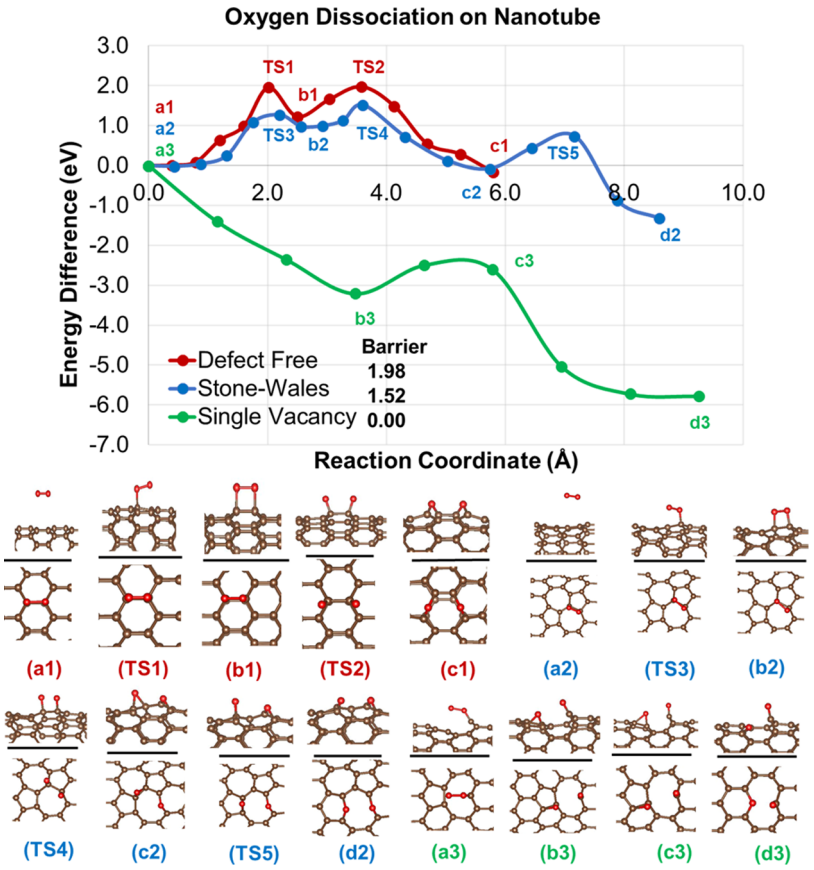

Figure 5. Calculated oxygen dissociation pathways on defect-free, SW-defected, and SV-defected (12,0) zigzag carbon nanotubes at the PBE level. The side-view structures are shown at the top and the top views are shown at the bottom. Note: only local structures are shown and the colors for the defective and normal carbon atoms are consistent.

(b2 in Figure 4) take places on the two carbon atoms between the two seven-membered ring, and the barrier is calculated to be 1.50 eV, which is ~1.50 eV less than the energy barrier on defect-free graphene. Again, the two unpaired electrons in the O_2 adsorbate are paired by surface carbon atoms in this step to form b2 and there are no unpaired electrons for the first transition state. The energy barrier for the formation of an epoxide intermediate (c2 in Figure 4) is also predicted to be 1.50 eV smaller than that on defect-free graphene. For the second transition state (ts4 in Figure 4), approximately a total of 0.4 unpaired electrons are predicted on the two oxygen adatoms per unit cell. The third step to form two ether groups is predicted to be the rate-determining step for the overall reaction. This step breaks two epoxy C−O bonds followed by oxygen transfer leading to the formation of two ether groups. One of the two oxygen adatoms is predicted to have 0.1 unpaired electrons for the third transition state. The calculated energy barrier is 1.90 and 1.46 eV relative to the physisorbed structure and the reactant, respectively.

On the graphene with an SV defect, the calculated energy barrier is only 0.29 eV for the formation of an intermediate with two dangling C−O bonds with two bi-coordinated defective carbon atoms. The transition state is only 0.06 eV higher than the reactant asymptote. No energy barrier is found for the formation of an ether group through a dangling C−O intermediate. Again, spin crossing is predicted for oxygen dissociation on SV-defected graphene and there are totally two unpaired electrons on the oxygen atoms and one bi-coordinated defective carbon atom for the transition state. The small energy barrier for O_2 dissociation on an SV site is consistent with the previous work using a cluster model for graphene and a mixed quantum mechanics/molecular mechanics (QM/MM) method, where the high-level calculations were performed at the B3LYP/6-31G level and the low-level system was calculated using a universal molecular mechanics force field.[67]

The dissociation of O_2 on defect-free carbon nanotubes is predicted to be a thermally neutral reaction including two steps (Figure 5). Again, the first process is to form an intermediate with a C−O−O−C group on the exterior wall. This step also includes a spin crossing from a triplet to a single potential energy surface with an energy barrier of 1.98 eV. The energy needed to overcome the second transition state to form ethers is comparable to the first one. Each oxygen adatom has 0.5 unpaired electrons for the second transition state. The energy barrier for the overall oxygen dissociation is 0.8 eV smaller than that on defect-free graphene. The calculated activation energy is slightly larger than that on the (8,0) single-walled carbon nanotube,[39] where an energy barrier of 1.61 eV was predicted with PBE. It is important to note that the formation of two epoxy groups' epoxide was previously predicted in the dissociation of O_2;[39] the formation of two ether groups is predicted to be more favorable in the current work.

Oxygen dissociation on the SW-defected carbon nanotube is exothermic for three elementary steps like the SW-defected graphene. Again, oxygen chemisorption passes through a first intermediate including a peroxyl group followed by a second intermediate including an epoxy and an ether group before the

https://doi.org/10.1021/acs.jpcc.1c06741
J. Phys. Chem. C XXXX, XXX, XXX−XXX

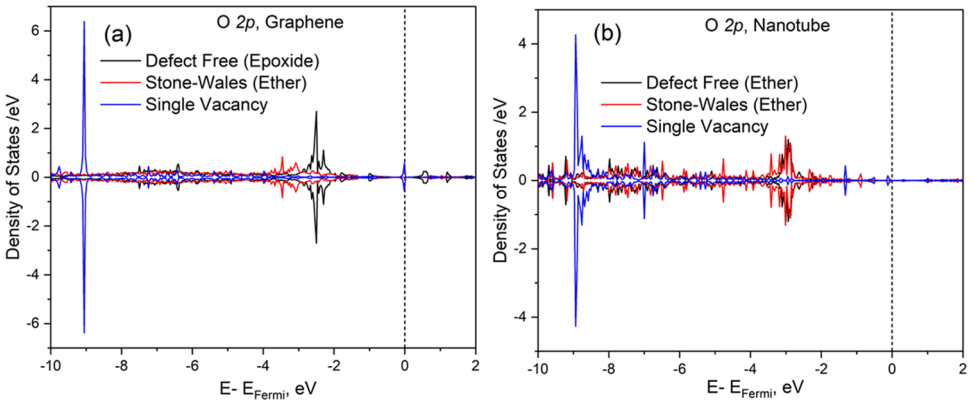

Figure 6. Projected density of states of O 2p orbitals in the products of atomic adsorption on defect-free, SW-defected, and SV-defected graphene (a) and carbon nanotube (b) at the PBE level. The structures correspond to Figure 1a,1c,g–i. The Fermi energy is shifted to 0.

final stabilization step to form two ether groups. The transition state for the second step has the highest energy with an energy barrier of 1.52 eV relative to the O_2 physisorbed structure. The energy barrier is 1.46 eV relative to the reactant. Approximately, 0.1 electrons are predicted on each of the oxygen adatoms for the first transition state; the second and the third transition states are predicted to be singlets with no unpaired electrons.

On the SV-defected nanotube, the dissociation should readily occur without an energy barrier. This is generally consistent with that on the graphene with an SV defect, as shown above. The process takes place through an intermediate including an epoxy group and a dangling carbonyl group on the exterior wall (b3 in Figure 5). The oxygen dissociation pathway on the SV defect carbon nanotube includes a spin crossing from the triplet to the singlet potential energy surface and the spin in the initial reactant (a3 in Figure 5) localizes on the two oxygen atoms.

Electronic Density of States. Figure 6 shows the projected density of states (DOSs) of the O 2p band in an energy window between −10 and 2 eV for atomic oxygen adsorption on different materials with and without a defect. On the defect-free graphene, a peak for the highest occupied state is calculated near −3.0 to −2.0 eV. The highest occupied O 2p band center in the ether group on the SW-defected graphene is shifted to the valence band by 0.45 eV as compared to that in the epoxide on the defect-free graphene. The predicted Fermi energies for both graphenes with an adsorbed O only differ by 0.05 eV. The O 2p band shift is in part due to more charge transfer to O from the SW-defective carbon atoms than that from the defect-free carbon atoms, predicted by the Bader charge analysis, where the O in an ether is more negative than the O in an epoxide. For the oxygen on the SV-defected graphene, a strong peak is found near −9.0 eV together with a weaker peak at the Fermi level. The DOSs of the 2p orbitals of the three C atoms bonded to the O (not shown) also show a strong peak near −9.0 eV and a weaker peak at the Fermi level. The symmetric DOS distribution near the Fermi level for both C and O 2p orbitals indicates that the covalent C−O bonds on an SV defect are formed by sharing the unpaired electron from the C around the vacancy and the O adsorbate. This is different from the covalent binding on a defect-free and an SW-defective site, where no unpaired electrons are predicted without the adsorbate of O.

The DOSs for the O 2p band on the carbon nanotube (Figure 6b) show similar peaks on both the defect-fee and SW-defected surfaces, where ether formation is favored for both. The oxygen 2p band on the SV-defected carbon nanotube is also similar to that on the SV-defected graphene. The binding on an SV site in the atomic oxygen adsorption is generally consistent on graphene and the nanotube. The DOSs for the atomic oxygen adsorption on graphite (Figure S6) show consistent peak positions with a broader width as compared to that on graphene.

Oxygen Adsorption Using Cluster Models. The DFT results for oxygen adsorption on graphene and zigzag carbon nanotubes using cluster models are shown in Figure 7. The

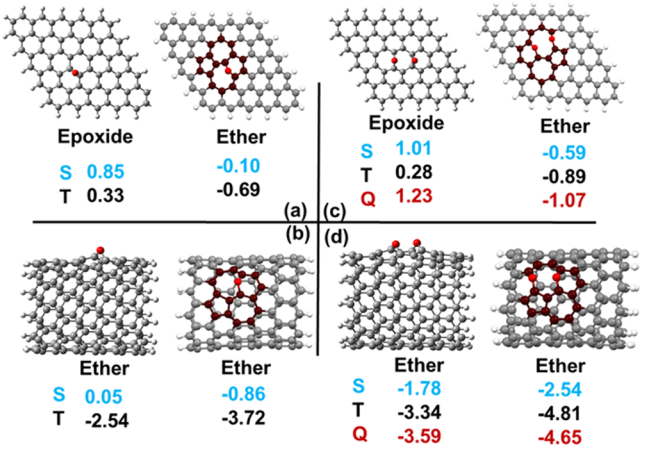

Figure 7. Optimized molecular structures and adsorption energies ($\Delta H_{0\,K}$) in eV for graphene and nanotube with cluster models at the M06-2X/6-311G(d,p) level. (a) and (c) for atomic and molecular adsorption on graphene; (b) and (d) for atomic and molecular oxygen adsorption on the nanotube; carbon atoms around a defect shown in purple and oxygen atoms shown in red. For the adsorption energy of atomic oxygen, one-half of the electronic energy of O_2 was selected for the adsorbate. S = singlet in blue, T = triplet in black; and Q = quintet in red.

graphene with H atoms attached to the terminal carbon atoms is predicted to be a closed-shell singlet for both defect-free and SW-defected clusters. The adducts with the adsorption of an O atom are predicted to be a triplet and the spin delocalizes on the edge carbon atoms (Figure 8). Similarly, the triplet state is predicted to be the ground state with atomic oxygen adsorption on the nanotube. The spin also delocalizes on the edge carbon atoms. Neither the epoxy nor the ether group has

https://doi.org/10.1021/acs.jpcc.1c06741
J. Phys. Chem. C XXXX, XXX, XXX−XXX

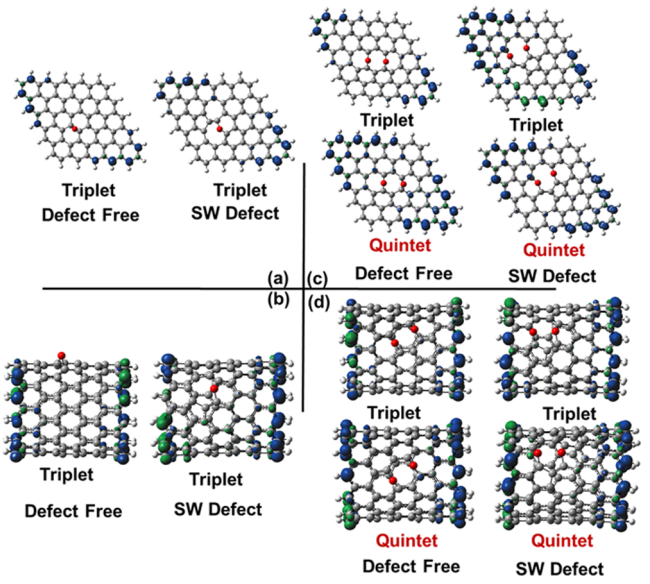

Figure 8. Calculated spin densities with an isovalue of 0.01 au at the M06-2X/6-311G(d,p) level. See Figure 7 for oxygen adsorption on different clusters.

unpaired electrons on the graphene and nanotube, which agrees well with the periodic DFT calculations. The cluster model has excess spin localized on the edges of the cluster. This most likely happens because the extended π system has a very low singlet−triplet (S−T) splitting before substitution of the oxygen as has been established for polyacenes up through heptacene.[68,69] As an example, the adiabatic S−T splitting in heptacene is 0.55 eV.[70] Our cluster model has a much larger extended π system, so the S−T splitting should be even smaller and more susceptible to perturbations. Addition of the triplet O atom perturbs the extended π system lowering the energy of the low-lying triplet so that it is now below the singlet state by ∼0.5 eV. This can happen because the excess spin density can localize on the edges of the cluster. In the periodic system, there are no edges for the spin to localize on, thus the triplet state does not localize in the periodic system.

Consistent with the periodic DFT results, an epoxide and an ether are predicted on defect-free and SW-defected graphene cluster models. The adsorption energies are predicted to be 0.33 eV and −0.69 eV, respectively. With respect to the nanotube, the formation of an ether is favored on both defect-free and SW-defected cluster models. Again, this is consistent with the periodic DFT calculations. The atomic oxygen adsorption energy on the SW-defected nanotube is predicted to be −3.72 eV, which is 1.18 eV more negative than that on the defect-free cluster model.

Dissociation of O_2 was also studied and the results are shown in Figure 7c,d for the cluster models of graphene and the nanotube, respectively. Again, the spin also delocalizes on the edge carbon atoms. An endothermic dissociation energy of 0.28 eV is predicted with the formation of two epoxy groups on the cluster model of defect-free graphene; the product is predicted to be a triplet. With the presence of a SW defect, the oxygen chemisorption is predicted to be exothermic by −1.07 eV leading to the formation of a quintet product including two ether groups in the seven-membered ring. The triplet state is predicted to be only 0.18 eV higher in energy than the quintet. For the cluster model of the nanotube, the dissociation of an O_2 molecule results in the formation of a quintet and a triplet for the defect-free and SW-defected cluster models. Again, the SW defect lowers the dissociative adsorption energy by 1.22 eV and a highly exothermic energy of −4.65 eV is predicted on the SW-defected nanotube.

The most favorable oxygen binding sites as well as the adsorption products are consistent using both cluster and periodic models. The adsorption energies on graphene using both models are comparable and more exothermic energies are predicted for the nanotube using cluster models. The larger exothermicity may be partially due to the presence of edge carbon atom in the clusters, which may exhibit specific chemical reactivities.[71] The consistent results with respect to the binding sites, adsorption products, and the more exothermicities on the SW defects using both models suggest that the NBO analysis from the cluster calculations can be used to better understand the nature of the binding in the periodic DFT calculations.

NBO Analysis. The hybridization properties as well as the weights of the hybrid orbital making a C−O bond from the NBO analysis on the clusters are shown in Table 1. We averaged those properties from the α and β spin orbitals as there is no extra spin on the C−O−C group and the values for both spin orbitals are generally consistent. The detailed hybridization properties on the α and β spin orbitals are shown in the Supporting Information. The epoxy C−O−C group on the defect-free graphene model arises from the interactions between $sp^{6.18}$ hybrid orbitals on the two C atoms and an $sp^{6.88}$ hybrid orbital on the O. For the ether on an SW defect, one C−O bond is from the interaction between an

Table 1. Hybridization Properties of C−O Bonds in the Epoxide and the Ether Formed on the Graphene and Nanotube from NBO Analysis Calculated at the M06-2X/6-311G(d,p) Level[a]

species	bond	h_C[b]	% p[c]	h_O[b]	% p[c]	wt$_C$ (%)[d]	wt$_O$ (%)[d]	δ_C[e]	δ_O[e]
graphene-epoxide	C1−O	$sp^{6.18}$	86.0%	$sp^{6.88}$	87.3%	35.3	64.7	0.22	−0.50
	C2−O	$sp^{6.19}$	86.0%	$sp^{6.90}$	87.3%	35.3	64.7	0.22	−0.50
graphene SW-ether	C1−O	$sp^{3.35}$	77.0%	$sp^{2.85}$	74.0%	32.8	67.2	0.34	−0.53
	C2−O	$sp^{3.47}$	77.7%	$sp^{2.98}$	74.9%	33.0	67.0	0.41	−0.53
nanotube ether	C1−O	$sp^{3.27}$	76.6%	$sp^{3.08}$	75.5%	33.5	66.5	0.35	−0.53
	C2−O	$sp^{3.28}$	76.6%	$sp^{3.08}$	76.0%	33.4	66.6	0.35	−0.53
nanotube SW-ether	C1−O	$sp^{3.51}$	77.8%	$sp^{3.08}$	75.5%	33.0	67.0	0.37	−0.54
	C2−O	$sp^{3.36}$	77.1%	$sp^{2.78}$	73.5%	33.2	66.8	0.34	−0.54

[a]Note: The composition, % p character, and the weight are the averaged values from α and β spin orbitals; the structures are shown in Figure 7. [b]Composition of the natural hybrids of C and O. [c]Percentage of the p character of the natural hybrids of C and O. [d]Weight of the natural hybrid orbitals to make a C−O bond. [e]Natural charge from natural population analysis (NPA)7.

https://doi.org/10.1021/acs.jpcc.1c06741
J. Phys. Chem. C XXXX, XXX, XXX−XXX

$sp^{3.35}$ hybrid orbital on the C and an $sp^{2.85}$ hybrid orbital on the O. The other C−O bond is formed via the interaction between an $sp^{3.47}$ hybrid orbital on the C and an $sp^{2.98}$ hybrid orbital on the O. Thus, the hybrid orbitals on C and O have more *p* character in the epoxide than that in the ether. For carbon nanotubes, the % *p* characters of the hybrid orbitals on both C and O are comparable to that on an SW-defected graphene and ether formation is favored in these cases. The % *p* characters of the hybrid orbitals on the O in the ether group on defect-free and SW-defected nanotubes are comparable with the difference of less than 2%. The significantly different weights of the hybrid orbitals of C and O suggest the C−O bonds in both the epoxide and the ether are polar covalent bonds. On graphene, the C−O bond in the ether on an SW defect is more polar than that in the epoxide formed on the defect-free surface. The polarities are comparable for the C−O bonds in the ether group on defect-free and SW-defected nanotubes.

The different adsorption energies with the formation of an ether and an epoxide on graphene correlate with less *p* character (more s character) on the C and O atoms in the ether group. The less 2p character (more 2s character) there is in the hybrid orbitals on the C and O, the stronger the C−O binding is predicted to be. The strain on the defective carbon atoms may also play an important role in the adsorption energy. For example, the presence of an SW defect increases the electronic energy of 5.32 and 3.66 eV per formula unit for the graphene (the model with 72C) and the nanotube (the model with 192C), respectively, in the periodic calculations. The defect-free carbon atoms are less strained and a weaker oxygen binding with them is predicted as compared to the binding with SW-defective carbon atoms on nanotubes (Figure 1), although ether formation is favored on both and the 2s character in the hybrid orbitals is comparable.

CONCLUSIONS

Plane-wave density functional theory has been used to study oxygen adsorption on the SW-defected and SV-defected graphene, graphite, and zigzag single-walled carbon nanotubes to compare to the adsorption behavior on defect-free materials. Atomic oxygen adsorption on defect-free graphene and graphite leads to the formation of a stable epoxide-like structure. In comparison, an ether-like structure is predicted on the exterior wall of carbon nanotubes and SW-defected materials. An SV site is predicted to be the most reactive for atomic oxygen adsorption. The chemisorption of O_2 is endothermic on defect-free graphene and graphite and slightly exothermic on the defect-free nanotube. O_2 chemisorption is exothermic on the defected materials. The presence of an SW defect lowers the energy barriers by ∼0.90 and 0.50 eV for O_2 chemisorption on the graphene and the nanotube. The formation of a peroxyl C−O−O−C group plays an important role for the dissociation. There is generally no energy barrier for O_2 dissociation on the SV-defected graphene and nanotube.

On graphene, the more reactive SW defect toward O adsorption is mostly due to the strained defective carbon atoms being able to donate more electrons to an O to release the epoxide ring strain to form an ether than the defect-free carbon atoms. The more 2s character in the hybrid orbitals in an ether than in an epoxide makes the C−O bond stronger in the ether. Stronger C−O binding on an SW-defective carbon nanotube than on a defect-free nanotube is in part due to the SW defect having more flexibility to release the epoxide ring strain to form an ether although ether formation is favored on both and the 2s character in the two ethers is comparable.

The calculations show that graphene is slightly more reactive than multilayer graphite in terms of oxygen adsorption. The presence of curvature increases the reactivity of defect-free materials. Impurities can be formed spontaneously on SV-defected carbonaceous materials as O_2 dissociation readily occurs on an SV defect. In catalytic reactions involving oxygen for carbonaceous materials as the catalyst or as a support, gas-phase O_2 can be activated by an SW defect under mild conditions, whereas defect-free carbon atoms on the planar graphene and graphite are generally inert for oxygen activation.

ASSOCIATED CONTENT

Supporting Information

The Supporting Information is available free of charge at https://pubs.acs.org/doi/10.1021/acs.jpcc.1c06741.

> Complete ref 58. Figures: computational models for periodic calculations; atomic oxygen adsorption on the different graphene layers; additional configurations and adsorption energies for atomic oxygen and molecular oxygen adsorption; configurations and energetics for the physisorption of molecular oxygen; projected DOS for the oxygen 2p band on graphite; atomic oxygen adsorption energies on a larger cluster for graphene and a nanotube. Table: calculated bond distances and bond angles of the products via atomic oxygen adsorption. Detailed NBO analysis results on α and β spin orbitals. Cartesian coordinates for the optimized geometries and electronic energies for the calculations using cluster models (PDF)

AUTHOR INFORMATION

Corresponding Authors

Zongtang Fang − *Biological and Chemical Science and Engineering Department, Idaho National Laboratory, Idaho Falls, Idaho 83415, United States;* orcid.org/0000-0001-6034-1083; Email: zongtang.fang@inl.gov

Eric J. Dufek − *Energy Storage and Advanced Transportation Department, Idaho National Laboratory, Idaho Falls, Idaho 83415, United States;* orcid.org/0000-0003-4802-1997; Email: eric.dufek@inl.gov

Authors

Lan Li − *Micron School of Materials Science and Engineering, Boise State University, Boise, Idaho 83725, United States; Center for Advanced Energy Studies, Idaho Falls, Idaho 83401, United States*

David A. Dixon − *Department of Chemistry and Biochemistry, The University of Alabama, Tuscaloosa, Alabama 35487, United States;* orcid.org/0000-0002-9492-0056

Rebecca R. Fushimi − *Biological and Chemical Science and Engineering Department, Idaho National Laboratory, Idaho Falls, Idaho 83415, United States;* orcid.org/0000-0002-7570-0234

Complete contact information is available at: https://pubs.acs.org/10.1021/acs.jpcc.1c06741

Notes

The authors declare no competing financial interest.

https://doi.org/10.1021/acs.jpcc.1c06741
J. Phys. Chem. C XXXX, XXX, XXX−XXX

■ ACKNOWLEDGMENTS

The authors acknowledge the support of the INL Laboratory Directed Research & Development (LDRD) Program under DOE Idaho Operations Office Contract No. DE-AC07-05ID14517. D.A.D. also thanks the Robert Ramsay Fund at The University of Alabama. The authors are grateful to Dr. Rakesh Batchu and Dr. William E. Windes for their comments on the computational results. This research made use of the resources of the High-Performance Computing Center at the Idaho National Laboratory, which is supported by the Office of Nuclear Energy of the U.S. Department of Energy and the Nuclear Science User Facilities under Contract No. DE-AC07-05ID14517. Accordingly, the U.S. Government retains a nonexclusive, royalty-free license to publish or reproduce the published form of this contribution, or allow others to do so, for U.S. Government purposes.

■ REFERENCES

(1) Mishra, A. K.; Ramaprabhu, S. Carbon Dioxide Adsorption in Graphene Sheets. *AIP Adv.* **2011**, *1*, No. 032152.
(2) Sui, Z.-Y.; Cui, Y.; Zhu, J.-H.; Han, B.-H. Preparation of Three-Dimensional Graphene Oxide-Polyethylenimine Porous Materials as Dye and Gas Adsorbents. *ACS Appl. Mater. Interfaces* **2013**, *5*, 9172−9179.
(3) Li, W.; Han, C.; Liu, W.; Zhang, M.-H.; Tao, K.-Y. Expanded Graphite Applied in the Catalytic Process as a Catalyst Support. *Catal. Today* **2007**, *125*, 278−281.
(4) Li, Y. F.; Guo, M. Q.; Yin, S. F.; Chen, L.; Zhou, Y. B.; Qiu, R. H.; Au, C. T. Graphite as a Highly Efficient and Stable Catalyst for the Production of Lactones. *Carbon* **2013**, *55*, 269−275.
(5) Yu, I. K. M.; Xiong, X.; Tsang, D. C. W.; Ng, Y. H.; Clark, J. H.; Fan, J.; Zhang, S.; Hu, C.; Ok, Y. S. Graphite Oxide- and Graphene Oxide-Supported Catalysts for Microwave-Assisted Glucose Isomerization in Water. *Green Chem.* **2019**, *21*, 4341−4353.
(6) Asenbauer, J.; Tobias, E.; Kuenzel, M.; Kazzazi, A.; Chen, Z.; Bresser, D. The Success Story of Graphite as a Lithium-Ion Anode Material − Fundamentals, Remaining Challenges, and Recent Developments Including Silicon (Oxide) Composites. *Sustainable Energy Fuels* **2020**, *4*, 5387−5416.
(7) Tingaev, M. I.; Belenkov, E. A. Hybrid sp^2+sp^3 Carbon Phases Created from Carbon Nanotubes. *J. Phys.: Conf. Ser.* **2017**, *917*, No. 032013.
(8) Tingaev, M. I.; Belenkov, E. A. Carbon Materials Formed by Polymerization of C20 and C24 Fullerites. *J. Phys.: Conf. Ser.* **2018**, *1124*, No. 022011.
(9) Falcao, E. H. L.; Wudl, F. Carbon Allotropes: Beyond Graphite and Diamond. *J. Chem. Technol. Biotechnol.* **2007**, *82*, 524−531.
(10) Dai, H. J. Carbon nanotubes: Synthesis, Integration, and Properties. *Acc. Chem. Res.* **2002**, *35*, 1035−1044.
(11) Sengupta, R.; Bhattacharya, M.; Bandyopadhyay, S.; Bhowmick, A. K. A Review on the Mechanical and Electrical Properties of Graphite and Modified Graphite Reinforced Polymer Composites. *Prog. Polym. Sci.* **2011**, *36*, 638−670.
(12) Liu, Y.; Sun, K.; Cui, X.; Li, B.; Jiang, J. Defect-Rich, Graphene Like Carbon Sheets Derived from Biomass as Efficient Electrocatalysts for Rechargeable Zinc−Air Batteries. *ACS Sustainable Chem. Eng.* **2020**, *8*, 2981−2989.
(13) Wang, W.; Shang, L.; Chang, G. J.; Yan, C. Y.; Shi, R.; Zhao, Y. X.; Waterhouse, G. I. N.; Yang, D. J.; Zhang, T. R. Intrinsic Carbon Defect-Driven Electrocatalytic Reduction of Carbon Dioxide. *Adv. Mater.* **2019**, *31*, No. 1808276.
(14) Jiang, H.; Gu, J.; Zheng, X.; Liu, M.; Qiu, X.; Wang, L.; Li, W.; Chen, Z.; Ji, X.; Li, J. Defect-Rich and Ultrathin N doped Carbon Nanosheets as Advanced Trifunctional Metal-Free Electrocatalysts for the ORR, OER and HER. *Energy Environ. Sci.* **2019**, *12*, 322−333.
(15) Yeung, C. S.; Chen, Y. K.; Wang, Y. A. Defected and Substitutionally Doped Nanotubes: Applications in Biosystems, Sensors, Nanoelectronics, and Catalysis. In *Carbon Nanotubes − Growth and Applications*; Naraghi, M., Ed.; InTech: Croatia, 2011; pp 97−132.
(16) Lu, D.; Wu, D.; Jin, J.; Chen, L. Defect-Induced Catalysis toward the Oxygen Reduction Reaction in Single-Walled Carbon Nanotube: Nitrogen Doped and Non-Nitrogen Doped. *Electrochim. Acta* **2016**, *215*, 66−71.
(17) Gewirth, A. A.; Varnell, J. A.; DiAscro, A. M. Nonprecious Metal Catalysts for Oxygen Reduction in Heterogeneous Aqueous Systems. *Chem. Rev.* **2018**, *118*, 2313−2339.
(18) Banhart, F.; Kotakoski, J.; Krasheninnikov, A. V. Structural Defects in Graphene. *ACS Nano* **2011**, *5*, 26−41.
(19) Yang, G.; Li, L.; Lee, W. B.; Ng, M. C. Structure of Graphene and Its Disorders: A Review. *Sci. Technol. Adv. Mater.* **2018**, *19*, 613−648.
(20) Ali, S.; Liu, T. F.; Lian, Z.; Li, B.; Su, D. S. The Effect of Defects on the Catalytic Activity of Single Au Atom Supported Carbon Nanotubes and Reaction Mechanism for CO Oxidation. *Phys. Chem. Chem. Phys.* **2017**, *19*, 22344−22354.
(21) Arunajatesan, V.; Chen, B.; Möbus, K.; Ostgard, D. J.; Tacke, T.; Wolf, D. In *Carbon Materials for Catalysis*; Serp, P.; Figueiredo, J. L., Eds.; John Wiley & Sons, Inc., 2008; pp 535−572.
(22) Auer, E.; Freund, A.; Pietsch, J.; Tacke, T. Carbons as Supports for Industrial Precious Metal Catalysts. *Appl. Catal., A* **1998**, *173*, 259−271.
(23) Gerber, I. C.; Serp, P. A. A Theory/Experience Description of Support Effects in Carbon-Supported Catalysts. *Chem. Rev.* **2020**, *120*, 1250−1349.
(24) Su, D. S.; Maksimova, N. I.; Mestl, G.; Kuznetsov, V. L.; Keller, V.; Schlögl, R.; et al. Oxidative Dehydrogenation of Ethylbenzene to Styrene Over Ultra-Dispersed Diamond and Onion-like Carbon. *Carbon* **2007**, *45*, 2145.
(25) Su, D. S.; Maksimova, N.; Delgado, J. J.; Keller, N.; Mestl, G.; Ledoux, M. J.; Schlogl, R. Nanocarbons in Selective Oxidative Dehydrogenation Reaction. *Catal. Today* **2005**, *102−103*, 110−114.
(26) Ma, R.; Lin, G.; Zhou, Y.; Liu, Q.; Zhang, T.; Shan, G.; Yang, M.; Wang, J. A Review of Oxygen Reduction Mechanisms for Metal-Free Carbon-Based Electrocatalysts. *npj Comput. Mater.* **2019**, *5*, No. 78.
(27) Yu, D. S.; Nagelli, E.; Du, F.; Dai, L. M. Metal-Free Carbon Nanomaterials Become More Active than Metal Catalysts and Last Longer. *J. Phys. Chem. Lett.* **2010**, *1*, 2165−2173.
(28) Dai, L.; Xue, Y.; Qu, L.; Choi, H. J.; Baek, J. B. Metal-Free Catalysts for Oxygen Reduction Reaction. *Chem. Rev.* **2015**, *115*, 4823−4892.
(29) Atamny, F.; Blöcker, J.; Henschke, B.; Schlögl, R.; Schedel-Niedrig, T.; Keil, M.; Bradshaw, A. M. Reaction of Oxygen with Graphite: X-Ray Absorption Spectroscopy of Carbonaceous Materials. *J. Phys. Chem. A* **1992**, *96*, 4522−4526.
(30) Sorescu, D. C.; Jordan, K. D.; Avouris, P. Theoretical Study of Oxygen Adsorption on Graphite and the (8,0) Single-Walled Carbon Nanotube. *J. Phys. Chem. B* **2001**, *105*, 11227.
(31) Dag, S.; Gulseren, O.; Yildirim, T.; Ciraci, S. Oxygenation of Carbon Nanotubes: Atomic Structure, Energetics, and Electronic Structure. *Phys. Rev. B* **2003**, *67*, No. 165424.
(32) Chan, S. P.; Chen, G.; Gong, X. G.; Liu, Z. F. Oxidation of Carbon Nanotubes by Singlet O_2. *Phys. Rev. Lett.* **2003**, *90*, No. 086403.
(33) Lee, S. M.; Lee, Y. H.; Hwang, Y. G.; Hahn, J. R.; Kang, H. Defect-Induced Oxidation of Graphite. *Phys. Rev. Lett.* **1999**, *82*, 217−220.
(34) Liu, J.; Liang, T.; Wang, C.; Lai, W. Oxygen Adsorption and CO Desorption Behavior of B- and N-doped Vacancy Defected Nuclear Graphite by DFT Study. *RSC Adv.* **2017**, *7*, 3257−3264.
(35) Perdew, J. P.; Burke, K.; Ernzerhof, M. Generalized Gradient Approximation Made Simple. *Phys. Rev. Lett.* **1996**, *77*, 3865−3868.
(36) Kresse, G.; Furthmüller, J. Efficiency of Ab-Initio Total Energy Calculations for Metals and Semiconductors Using a Plane-Wave Basis Set. *Comput. Mater. Sci.* **1996**, *6*, 15−50.

https://doi.org/10.1021/acs.jpcc.1c06741
J. Phys. Chem. C XXXX, XXX, XXX−XXX

(37) Kresse, G.; Hafner, J. Ab Initio Molecular Dynamics for Open-Shell Transition Metals. *Phys. Rev. B* **1993**, *48*, 13115−13118.
(38) Kresse, G.; Hafner, J. Ab Initio Molecular Dynamics for Liquid Metals. *Phys. Rev. B* **1993**, *47*, 558−561.
(39) Ni, S.; Li, Z. Y.; Yang, J. L. Oxygen Molecule Dissociation on Carbon Nanostructures with Different Types of Nitrogen Doping. *Nanoscale* **2012**, *4*, 1184−1189.
(40) Mehmood, F.; Pachter, R.; Lu, W.; Boeckl, J. Adsorption and Diffusion of Oxygen on Single-Layer Graphene with Topological Defects. *J. Phys. Chem. C* **2013**, *117*, 10366−10374.
(41) Klimeš, J.; Bowler, D. R.; Michaelides, A. Chemical Accuracy for the Van der Waals Density Functional. *J. Phys.: Condens. Matter* **2010**, *22*, No. 022201.
(42) Harrison, W. A. *Electronic Structure and the Properties of Solids: The Physics of the Chemical Bond*; Freeman: San Fransisco, 1980.
(43) Henkelman, G.; Jónsson, H.; et al. A Climbing Image Nudged Elastic Band Method for Finding Saddle Points and Minimum Energy Paths. *J. Chem. Phys.* **2000**, *113*, 9901−9904.
(44) Henkelman, G.; Jónsson, H. Improved Tangent Estimate in the Nudged Elastic Band Method for Finding Minimum Energy Paths and Saddle Points. *J. Chem. Phys.* **2000**, *113*, 9978−9985.
(45) Bader, R. F. W. *Atoms in Molecules: A Quantum Theory*; Oxford University Press: New York, 1990.
(46) Tang, W.; Sanville, E.; Henkelman, G. A Grid-Based Bader Analysis Algorithm Without Lattice Bias. *J. Phys.: Condens. Matter* **2009**, *21*, No. 084204.
(47) Glendening, E. D.; Landis, C. R.; Weinhold, F. NBO 6.0: Natural bond orbital analysis program. *J. Comput. Chem.* **2013**, *34*, 1429−1437.
(48) Glendening, E. D.; Badenhoop, J. K.; Reed, A. E.; Carpenter, J. E.; Bohmann, J. A.; Morales, C. M.; Landis, C. R.; Weinhold, F. Theoretical Chemistry Institute, University of Wisconsin, Madison, WI, 2013. http://nbo6.chem.wisc.edu/.
(49) Weinhold, F. *Encyclopedia of Computational Chemistry*; In von Ragué Schleyer, P., Ed.; John Wiley & Sons: Chichester, U.K., 1998; Vol. 3, pp 1792−1811.
(50) Weinhold, F.; Landis, C. R. *Valency and Bonding: A Natural Bond Orbital Donor−Acceptor Perspective*; University Press: Cambridge, U.K, 2005.
(51) Reed, A. E.; Curtiss, L. A.; Weinhold, F. Intermolecular Interactions from A Natural Bond Orbital, Donor-Acceptor Viewpoint. *Chem. Rev.* **1988**, *88*, 899−926.
(52) Reed, A. E.; Weinstock, R. B.; Weinhold, F. Natural Population Analysis. *J. Chem. Phys.* **1985**, *83*, 735−746.
(53) Zhao, Y.; Truhlar, D. G. The M06 suite of Density Functionals for Main Group Thermochemistry, Thermochemical Kinetics, Noncovalent Interactions, Excited States, and Transition Elements: Two New Functionals and Systematic Testing of Four M06-class Functionals and 12 Other Functionals. *Theor. Chem. Acc.* **2008**, *120*, 215−241.
(54) Hehre, W. J.; Ditchfield, R.; Pople, J. A. Self-Consistent Molecular Orbital Methods. XII. Further Extensions of Gaussian-Type Basis Sets for Use in Molecular Orbital Studies of Organic Molecules. *J. Chem. Phys.* **1972**, *56*, 2257−2261.
(55) Dill, J. D.; Pople, J. A. Self-Consistent Molecular Orbitals Methods. XV. Extended Gaussian-Type Basis Sets for Lithium, Beryllium and Boron. *J. Chem. Phys.* **1975**, *62*, 2921−2923.
(56) Francl, M. M.; Pietro, W. J.; Hehre, W. J.; Binkley, J. S.; Gordon, M. S.; DeFrees, D. J.; Pople, J. A. Self-Consistent Molecular Orbital Methods. XXIII. A Polarization-Type Basis Set for Second-Row Elements. *J. Chem. Phys.* **1982**, *77*, 3654−3665.
(57) Ramos-Berdullas, N.; Perez-Juste, I.; Van Alsenoy, C.; Mandado, M. Theoretical Study of the Adsorption of Aromatic Units on Carbon Allotropes Including Explicit (empirical) DFT Dispersion Corrections and Implicitly Dispersion-Corrected Functionals: the Pyridine Case. *Phys. Chem. Chem. Phys.* **2015**, *17*, 575−587.
(58) Frisch, M. J.; Trucks, G. W.; Schlegel, H. B.; Scuseria, G. E.; Robb, M. A.; Cheeseman, J. R.; Scalmani, G.; Barone, V.; Petersson, G. A.; Nakatsuji, H. et al. *Gaussian 16*, revision A.03; Gaussian, Inc.: Wallingford, CT, 2016.
(59) Qi, X.; Guo, X.; Zheng, C. Density Functional Study the Interaction of Oxygen Molecule with Defect Sites of Graphene. *Appl. Surf. Sci.* **2012**, *259*, 195−200.
(60) Kroes, J. M. H.; Pietrucci, F.; Curioni, A.; Jaafar, R.; Gröning, O.; Andreoni, W. Atomic Oxygen Chemisorption on Carbon Nanotubes Revisited with Theory and Experiment. *J. Phys. Chem. C* **2013**, *117*, 1948−1954.
(61) Guang, H.; Aoki, M.; Tanaka, S.; Kohyama, M. Hole Doping by Adsorption of Oxygen on a Stone-Thrower-Wales Defect in Graphene. *Solid State Commun.* **2013**, *174*, 10−15.
(62) Giannozzi, P.; Car, R.; Scoles, G. Oxygen Adsorption on Graphite and Nanotubes. *J. Chem. Phys.* **2003**, *118*, 1003−1006.
(63) Xu, Y.-J.; Li, J.-Q. The Interaction of Molecular Oxygen with Active Sites of Graphite: A Theoretical Study. *Chem. Phys. Lett.* **2004**, *400*, 406−412.
(64) Larciprete, R.; Lacovig, P.; Gardonio, S.; Baraldi, A.; Lizzit, S. Atomic Oxygen on Graphite: Chemical Characterization and Thermal Reduction. *J. Phys. Chem. C* **2012**, *116*, 9900−9908.
(65) Barinov, A.; Malcioğlu, O. B.; Fabris, S.; Sun, T.; Gregoratti, L.; Dalmiglio, M.; Kiskinova, M. Initial Stages of Oxidation on Graphitic Surfaces: Photoemission Study and Density Functional Theory Calculations. *J. Phys. Chem. C* **2009**, *113*, 9009−9013.
(66) Carlsson, J. M.; Hanke, F.; Linic, S.; Scheffler, M. Two-Step Mechanism for Low-Temperature Oxidation of Vacancies in Graphene. *Phys. Rev. Lett.* **2009**, *102*, No. 166104.
(67) Allouche, A.; Ferro, Y. Dissociative Adsorption of Small Molecules at Vacancies on the Graphite (0001) Surface. *Carbon* **2006**, *44*, 3320−3327.
(68) Einholz, R.; Fang, T.; Berger, R.; Grüninger, P.; Früh, A.; Chasse, T.; Fink, R. F.; Bettinger, H. F. Heptacene: Characterization in Solution, in the Solid State, and in Films. *J. Am. Chem. Soc.* **2017**, *139*, 4435−4442.
(69) Chakraborty, H.; Shukla, A. Theory of Triplet Optical Absorption in Oligoacenes: From Naphthalene to Heptacene. *J. Chem. Phys.* **2014**, *141*, No. 164301.
(70) Hajgató, B.; Szieberth, D.; Geerlings, P.; De Proft, F.; Deleuze, M. S. A Benchmark Theoretical Study of the Electronic Ground State and of the Singlet-Triplet Split of Benzene and Linear Acenes. *J. Chem. Phys.* **2009**, *131*, No. 224321.
(71) Bellunato, A.; Arjmandi Tash, H.; Cesa, Y.; Schneider, G. F. Chemistry at the Edge of Graphene. *ChemPhysChem* **2016**, *17*, 785−801.

https://doi.org/10.1021/acs.jpcc.1c06741
J. Phys. Chem. C XXXX, XXX, XXX−XXX